Pergamon

0956-7151(93)E0002-K

Acta metall. mater. Vol. 42, No. 6, pp. 2069–2081, 1994

0956-7151/94 $7.00 + 0.00

CREEP AND FRACTURE IN MODEL NIOBIUM–ALUMINA LAMINATES UNDER SHEAR LOADING

X. WU[1,2], J. W. HOLMES[2] and A. K. GHOSH[1]

[1]Department of Materials Science and Engineering and [2]Department of Mechanical Engineering and Applied Mechanics, The University of Michigan, Ann Arbor, MI 48109, U.S.A.

(Received 8 April 1993; in revised form 28 August 1993)

Abstract—A simple experimental technique was developed to study the near-interface deformation and fracture behavior in ductile-phase-toughened brittle-matrix laminates subjected to elevated-temperature shear loading. In the study, specimens of Nb-foils bonded to Al_2O_3 blocks were subjected to shear loading parallel to the Nb/Al_2O_3 interfaces. The fracture path was controlled by the applied stress, the temperature and the thickness of the ductile Nb layers. At high shear stresses failure took place by brittle fracture within the Al_2O_3 phase with concurrent shear creep in the Nb, and multiple crack branching/arresting toward the interface. At lower stresses, shear-creep and ductile fracture within the Nb were the dominant damage modes. Shear deformation was found to localize along the mid-plane of the Nb, due to strengthening of the Nb adjacent to the interface via solid solution and precipitation resulting from interdiffusion. With thin 20 μm Nb-layers the fracture energy was low, similar to that found for pure Al_2O_3. Our findings suggest that the ductile-phase toughening of laminated brittle matrix composites depends critically on the thickness of the ductile phase. A concept of brittle-ductile transition to assist in the understanding of the toughness enhancement provided by ductile phase additions into a brittle matrix.

1. INTRODUCTION

In recent times, toughening concepts involving the introduction of ductile phases in brittle ceramic or intermetallic matrices are being examined [1–6]. While it has been demonstrated that some degree of toughening is possible at room temperature, the effect of the ductile phases on the high temperature strength and toughness have not been studied. Since the development of these materials are primarily for applications at elevated temperature, it is of interest to examine the role of ductile phase, its thickness and interface properties on the elevated temperature creep and fracture behaviors in brittle matrix composites. A critical factor affecting the toughness, strength, and creep resistance of ductile-phase reinforced composites is the nature of the interface.

Various experimental techniques have been developed to study the mechanical behavior of interfaces in bi-materials under different loading modes; many of these techniques involve combined normal and shear loading along the interface. The vast majority of the investigations to-date have, however, been conducted at room temperature. Ritchie *et al.* [7–9] used double-cantilever-beam and compact tension specimens to study the Mode-I interface fracture behavior of metal–glass and metal–ceramic systems under monotonic and cyclic loading. Charalambides *et al.* [10], Dalgleish *et al.* [11, 12], and Cao *et al.* [13] utilized 4-point bending of laminated bars to evaluate the effect of fracture mode mixity on interface fracture energy. The phase angle, $\Psi = \tan^{-1}(K_{II}/K_I)$, which specifies the mixity of Mode-I and Mode-II loading, was typically about 50°, and it can be varied by changing specimen dimension. Fiber push-out and pull-out tests have also been used for primarily shear (Mode-II) loading; however, these methods are not directly applicable to bimaterials containing a deformable phase, due to extensive plastic bending encountered near the interface. Other tests, having more complex loading conditions, include the bending of bi-material beams [14–16] and the peeling of thin films [17]. These tests have provided data on the interface fracture energies of several bi-material pairs, including the Nb/Al_2O_3 system. The measured interface fracture energies and crack path depend not only on the specific bi-material system and processing history, but also on many other factors, including crystal orientation [18–21], mode mixity [22–24], interface microstructure [25] and roughness [26], loading rate [18], loading pattern (cyclic vs monotonic) and environment [27].

As mentioned before, these tests do not address the case where one of the phases can undergo creep flow at elevated temperature. In the present paper we report on a plane-shear test, which was developed primarily for studying the elevated temperature creep and fracture behavior of bi-materials under a phase angle that is close to $\pi/2$ (i.e. predominantly shear loading). The technique, which uses a punch and die setup to apply shear loading parallel to interfaces in bi-materials, offers simplicity in both testing operation and specimen preparation. Using this approach, the creep and fracture behavior of

Nb/Al_2O_3 specimens (with different Nb-layer thicknesses) was studied under various applied stresses and temperatures. The primary goal of the work was to determine how the introduction of a ductile Nb layer and the near-interface chemistry influences crack path and fracture behavior of a brittle Al_2O_3 matrix. The results of these experiments also provide insight into the elevated temperature shear behavior of brittle matrix composites containing ductile phases.

2. EXPERIMENTAL

2.1. Specimen preparation

Laminated Nb/Al_2O_3 specimens were used as a model brittle–ductile material system. The specimens were prepared by diffusion bonding of Nb foils sandwiched between three rectangular Al_2O_3 blocks (stacking sequence: $Al_2O_3/Nb/Al_2O_3/Nb/Al_2O_3$). High-purity α-Al_2O_3 plates (Coors AD-999; 99.9% Al_2O_3 with approximately 5% porosity) with dimensions of 25 mm × 25 mm × 4.5 mm, were metallographically polished on their bonding faces with 6 μm diamond paste, followed by ultrasonic cleaning in acetone for 2 h. Prior to diffusion bonding, the thickness of each Nb foil was either 127 or 25 μm. The specimens were diffusion bonded at 1600°C for 2 h in flowing argon under a ram pressure of 7 MPa. After bonding, the specimens were cooled at a rate of 5°C per min to below 600°C. The residual stress at the interface are expected to be small since the coefficient of thermal expansion of Nb (7.88×10^{-6}/K [28]) and Al_2O_3 (8.3×10^{-6}/K, from Coors) are close. The diffusion bonding was performed on a conventional mechanical testing system (Model 4507, Instron Corp., Canton, Mass.), that was fitted with a tungsten-mesh resistance furnace inside an environmental chamber (Model M60-3 × 8-W-D-02M2-A-20, Centorr Furnaces, Nashua, N.H.), and graphite loading rams. Prior to diffusion bonding, the chamber was first pumped down to below 10^{-4} torr vacuum and then filled with pre-purified argon (99.998%). The oxygen partial pressure was monitored continuously with an oxygen analyzer (Model FA30111A, Delta F Corp., Woburn, Mass), and found to be below 2 ppm during diffusion bonding.

After diffusion bonding the thickness of the Nb-layers decreased to approximately 100 μm or 20 μm (for initial foil thicknesses of 127 and 25 μm, respectively). The Nb grain size was approximately 100 μm in the thickness direction and about 300 μm along the interface direction (the Nb grain boundaries were perpendicular to the Nb/Al_2O_3 interfaces). The grain size of the as-received Al_2O_3 was about 5 μm, with no appreciable change found after diffusion bonding.

The diffusion-bonded blocks were cut into rectangular specimens, with a height of 5 mm, a width of 3.5 mm and a total length of about 14 mm. To provide a known initial defect for crack propagation, some of the specimens were notched near the interfaces (within the Al_2O_3, see Fig. 1). The notch depth

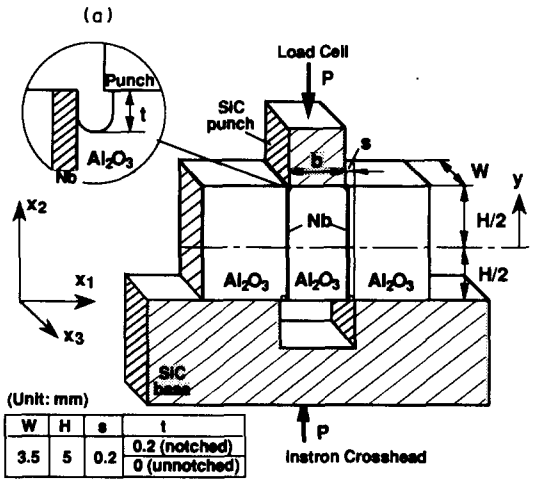

Fig. 1. (a) Schematic of experimental set-up and specimen geometry; (b) photograph of the loading ram–specimen–die base arrangement within the furnace.

was about 0.2 mm and the width about 0.15 mm. The locations of the notches were chosen based upon the results obtained from several preliminary experiments, which showed that cracks tended to initiate from contact with the tool edges. Locating the notches at the contact points of the punch and the SiC-base provided better control of the crack initiation sites. Since the primary goal of the experiments was to determine how the ductile Nb phase influenced the crack path in the Al_2O_3, an initially sharp crack was not necessary since cracks could be readily started at the notch tips.

2.2. Shear test

A punch-die set-up was used to test the specimens in shear. The experimental arrangement is shown in Fig. 1(a, b). The loading fixture consisted of a SiC-punch of 3.8 mm width, and a SiC die-base with a groove-width of 4.2 mm. To minimize the introduction of normal stresses along the Nb/Al_2O_3 interfaces, caused by bending of the specimen, the clearance between the contact points of the punch and die-base were maintained extremely small [see s in Fig. 1(a)] in comparison to the specimen height (5 mm). Experimental results shown later in this paper indicate that the predominant loading is shear parallel to the interface.

The shear experiments were performed using the same mechanical testing system and environmental chamber that was used for diffusion bonding. To accurately locate the specimen in the test fixture, the specimen was viewed through an optical microscope and glued with a bead of superglue to the die-base and punch. After placing the loading fixture and specimen in the load frame, a preload of 50 N (about 1.5 MPa) was maintained on the punch to prevent movement of the assembly during specimen heating and subsequent application of the punch load. (Note that the superglue burns off during first stage of heating at 400°C in vacuum.) The chamber was next back-filled with argon and maintained at 1 atm pressure, after which a constant heating rate of 20°C/min was maintained until the test temperature was reached. During the experiments, the specimen temperature was controlled to within $\pm$ 1°C of the particular test temperature. Upon completion of each test, the furnace was immediately turned off and the specimen was cooled to below 800°C within 1 min, to minimize possible microstructural changes in the specimens.

Two testing schedules were used in the experiments: (1) *constant displacement-rate* and (2) *constant load.* In the constant displacement-rate experiments, 100 μm Nb/Al_2O_3 specimens were loaded at a punch speed of 0.1 mm/min and at 1300°C; using separate specimens, the evolution of microstructural damage with increasing strain was determined by stopping tests at displacements of 0.12, 0.20, 0.27, and 0.31 mm, respectively. As a comparison, 20-μm Nb/Al_2O_3 specimens and pure Al_2O_3 specimens (without Nb interlayer) were tested under the same conditions used for the experiments with 100-μm Nb/Al_2O_3 specimens. In all these tests the notched specimen geometry was used (see Fig. 1). In the constant load experiments, the mean shear stress along the interfaces was maintained in the range of 5–30 MPa, which was lower than the peak stresses developed in the constant displacement-rate tests described above. Preliminary experiments indicated that under these low stresses the Nb layer showed significant creep deformation, with only limited creep or microstructural damage occurring within the Al_2O_3 or along the interface, even when notched specimens were used. Since the notches did not influence the creep behavior or microstructural damage process within the Nb layers, which was the main focus of the constant load experiments, the simpler unnotched specimens were utilized in the constant load experiments. These tests were also interrupted at designated times or displacements, so that the microstructural damage and the Nb local creep strain could be assessed.

During the experiments, a computer data acquisition system recorded the time t, load P, and displacement d. The load and displacement signals were obtained from a standard 10 kN load cell and crosshead motion, respectively. The total crosshead displacement includes the elastic deformation of the entire loading train, which is constant under a fixed load. Thus, during the constant load creep experiments, the change in displacement can be attributed to plastic deformation and microstructural damage occurring within the specimen. For constant displacement-rate experiments, specimen displacement can be reasonably estimated by subtracting the elastic displacement of the load frame and test fixtures from the total displacement. (The load frame and test fixture compliance was estimated from the load–displacement relation obtained without a specimen.) Using the following relationships and the measured data sets of (P, d, t) found from the constant load creep tests, the mean values of shear strain γ, strain rate $\dot{\gamma}$, and shear stress τ can be estimated: $\gamma = d/\delta$ (where δ is the Nb thickness), $\dot{\gamma} = \Delta\gamma/\Delta t$, and $\tau = P/(2HW)$, (see Fig. 1).

2.3. *Microstructural and compositional examination*

After testing, the fracture path and microstructural damage in the specimens was determined by optical microscopy and scanning electron microscopy. The chemical composition was determined by microprobe analysis (MBX-MICROBEAM, Cameca, Stamford, Conn.), and the phases were identified by use of an X-ray diffractometer (Rigaku Goniometer and Rotaflex, D/MAX-B system, Rigaku Corp., Tokyo). These measurements were compared with those from virgin specimens. In addition, the variation in microhardness across the 100 μm Nb-layer in virgin specimens was characterized by room temperature microhardness measurements using a Knoop indenter.

3. EXPERIMENTAL RESULTS AND DISCUSSION

In this section we first describe the mechanical behavior and microstructural investigation of damage modes found for the specimens with 100 μm thick Nb-layers (hereafter referred to as the thick layers). The behavior of these specimens is contrasted with that found for specimens that had thinner (20 μm) Nb-layers. Finally, the overall shear-fracture process for the bi-material specimens is summarized.

3.1. *Constant displacement-rate experiments: high stresses behavior*

3.1.1. Mechanical behavior. Figure 2 shows typical load vs displacement curves for 100 μm Nb/Al_2O_3 specimens that were interrupted at different stages of deformation. For these experiments, the test temperature was 1300°C and the punch speed was 0.1 mm/min. The loading curves exhibit nearly linear behavior in the early stages of loading. The slope of the curves decrease until the ultimate load is reached, after which the load decreases until failure; the decreasing slope is attributed to plastic deformation within the specimen. The scatter in the loading curves is believed to be a consequence of sample to sample

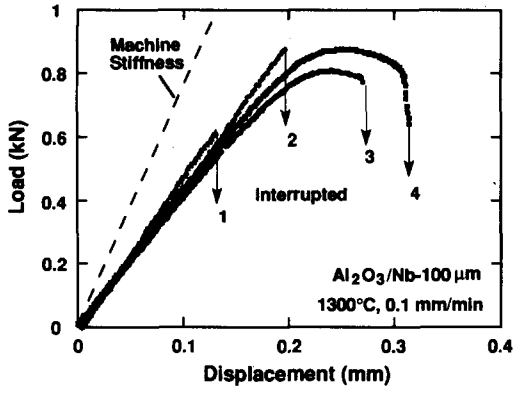

Fig. 2. Load vs total displacement curves for a set of interrupted experiments conducted at 1300°C under a constant punch displacement-rate of 0.1 mm/min. The results shown are for 100 μm Nb specimens. The stiffness of the machine without specimen is shown by the dashed line. The specimen displacement can be calculated by subtracting the machine's displacement from total displacement.

variation. It is important to note that the scatter is relatively small when compared with the displacement due to the machine compliance itself.

3.1.2. Damage process. Figure 3 shows the evolution of microstructural damage in specimens that were loaded at a constant displacement rate. Figure 4 shows the details of the damage that occurred within the Nb phase (the loading curves for these specimens are shown in Fig. 2, and marked 1–4, respectively). Two damage mechanisms were operating in parallel as the accumulated strain increased: (1) intergranular fracture within the Al_2O_3 in the vicinity of the Nb/Al_2O_3 interfaces (Fig. 3), and (2) shear creep and fracture within the Nb-layers (Fig. 4). The main crack initiated from the notch and propagated through the Al_2O_3 phase in an intergranular manner, which was verified by SEM. This main crack did not follow a path directly joining the two notches, rather, it was attracted toward the interface early in the deformation process [see Fig. 3(1, 2)]. It is believed that the plastically deforming Nb layer modifies the stress distribution in the loading direction by imposing shear traction directly along the mid-plane of the Nb layer; this can induce a local K_I-loading near the top and bottom of the specimens, as shown by the simple schematic in Fig. 3(b). Crack is then deflected at 45° to the interface, which is the direction of

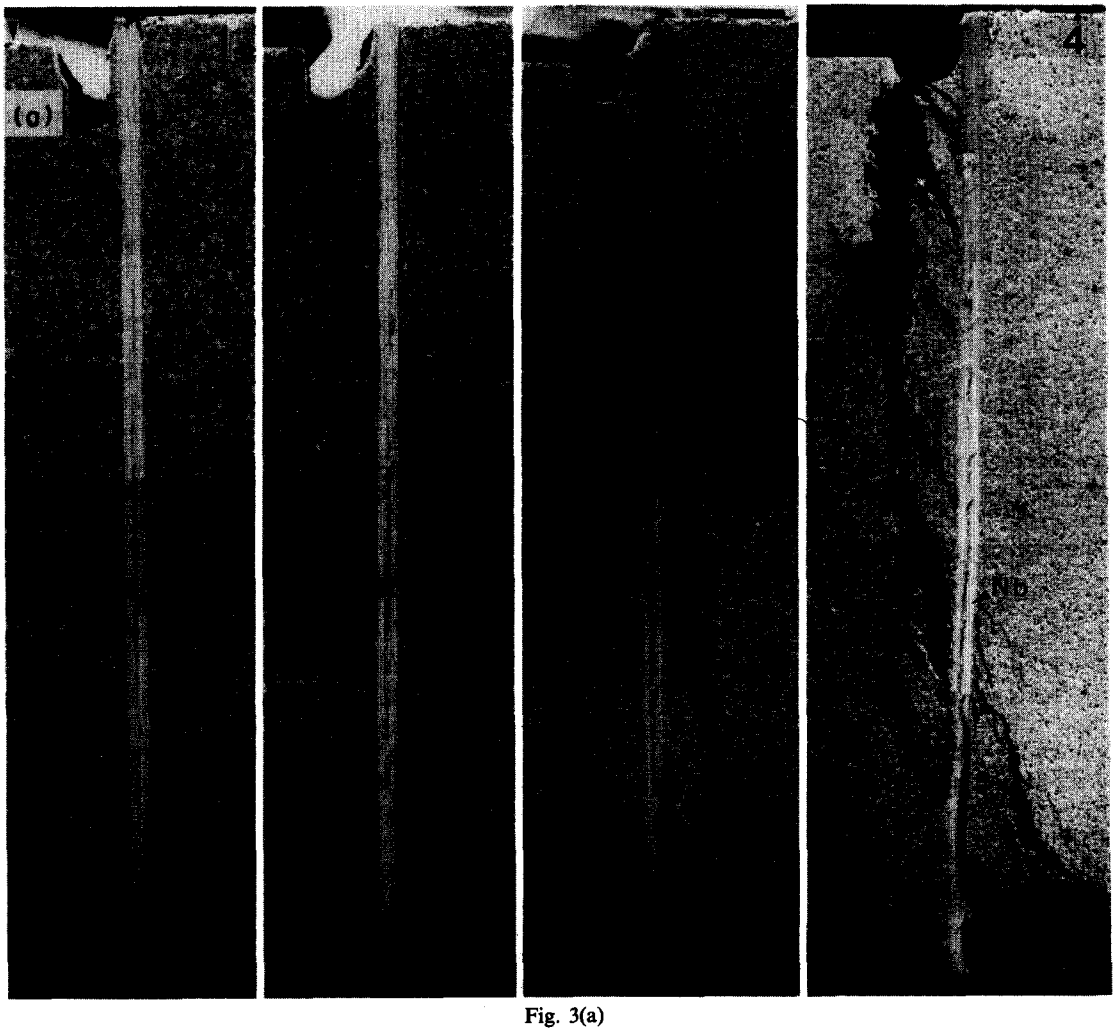

Fig. 3(a)

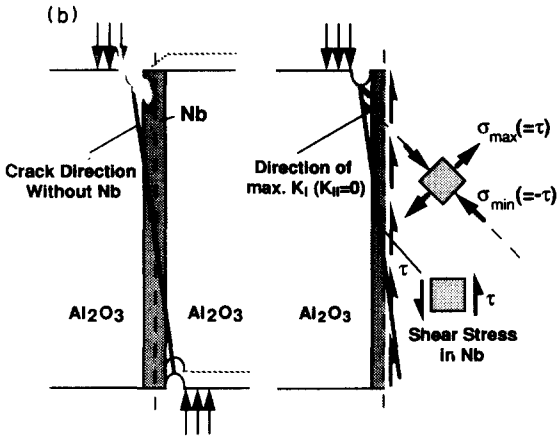

Fig. 3. (a) SEM micrographs of interrupted test specimens described in Fig. 2. Note the evolution of cracking with increasing punch displacement: (1) 0.13 mm; (2) 0.2 mm; (2) 0.27 mm; (2) 0.30 mm. (b) Schematic showing how shear in the ductile phase influences the crack path by branching to the Nb/Al_2O_3 interfaces.

highest local K_I/K_{II} ratio. As the crack approaches the interface, the higher interfacial strength and toughness retards the motion of this crack. This kind of crack deflection toward the interface is directly attributed to the shear deformation of Nb phase, and its arrest is a result of a "strong" interface. Continuously increasing load reactivates the main crack sufficiently to provide further propagation within the Al_2O_3 phase [see Fig. 3(3)]. The high strain rate sensitivity of Nb is believed to be responsible for its ability to transmit this high load to the Al_2O_3 phase. This periodic crack branching/arresting process continues until the stress-fields from the dominant cracks on either side of the ductile phase start to interact [see Fig. 3(4)]. When the two cracks from both top and bottom of the specimen merge near the middle of the specimen, the total applied load is carried primarily by the Nb layer, leading to specimen failure by local necking or tear-out of the Nb layer.

The attraction of cracks toward the interface in bi-materials has been reported by Rühle *et al.* [18] for Mode-I loading of Nb/Al_2O_3 specimens. In his experiments, Rühle observed that an indentation crack in the Al_2O_3 located adjacent to the interface had a tendency to propagate toward the interface. A continuous crack branching/attraction phenomenon under primarily far-field Mode-II loading has not been reported; such a phenomenon is closely related to the shear deformation that occurs when a ductile interlayer is embedded in a brittle matrix. When a main crack intersects the Nb/Al_2O_3 interface, plastic deformation of the Nb reduces the crack-tip stress intensity, preventing crack propagation through the Nb. Because of the very strong bond of the Nb/Al_2O_3 interface, the crack does not propagate along the interface.

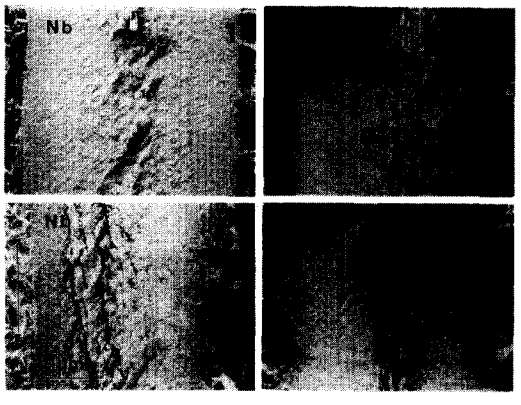

Fig. 4. Progressive damage development in the Nb layer for constant displacement-rate tests. The micrographs are enlarged from the central regions from Fig. 3(a).

In parallel with the development of cracking in the Al_2O_3, shear fracture or creep occurs simultaneously in the Nb layer. At an early stage of the experiment shear flow lines begin to develop in the Nb at an angle of 18–25° to the Nb/Al_2O_3 interfaces (see Fig. 4(1)). The angle decreases with an increase in the imposed displacement. These shear flow lines are located primarily in the central portion of the Nb layer. With increasing shear strain, the flow lines rotate and small cracks form. These small cracks link up to form a zigzag path along the length of the Nb layer (see Fig. 4). The small cracks are inclined at about 12–20° to the interface direction. Despite severe shear damage, portions of the central region of the Nb remained bonded, possibly due to rejoining, and continue to support the applied load. To summarize, at high applied stresses (above 40 MPa), ductile shear flow within the Nb layer and brittle multiple cracking of the Al_2O_3 contribute to the deformation of the composite.

3.2. Constant load test: constrained creep and fracture at low stresses

3.2.1. Mechanical behavior. Figure 5(a) shows the displacement vs time curves for representative constant load experiments conducted with the thick layer specimens. In Fig. 5(b), the steady-state creep rates, obtained from the slopes of the secondary stage of the creep curves, were plotted against the applied stresses for several temperatures from 1000 to 1300°C. Also shown in Fig. 5(b) are the creep data for the thin Nb specimens at 1200°C. The creep rates for these are two orders of magnitude lower than that for the thick layer specimens tested under the same conditions. The creep displacement and average creep rate measured from crosshead displacement were compared with the shear displacement of Nb layer obtained by examination of SEM micrographs (given in the next section); good agreement between these two measurements was obtained. Creep of Al_2O_3 at the relatively low stress and temperature, based on various sources (see a review by Cannon and Langdon [29]), is several orders of magnitude lower than that of Nb, and therefore negligible. Thus, shear creep in the Nb layers is responsible for the majority of the

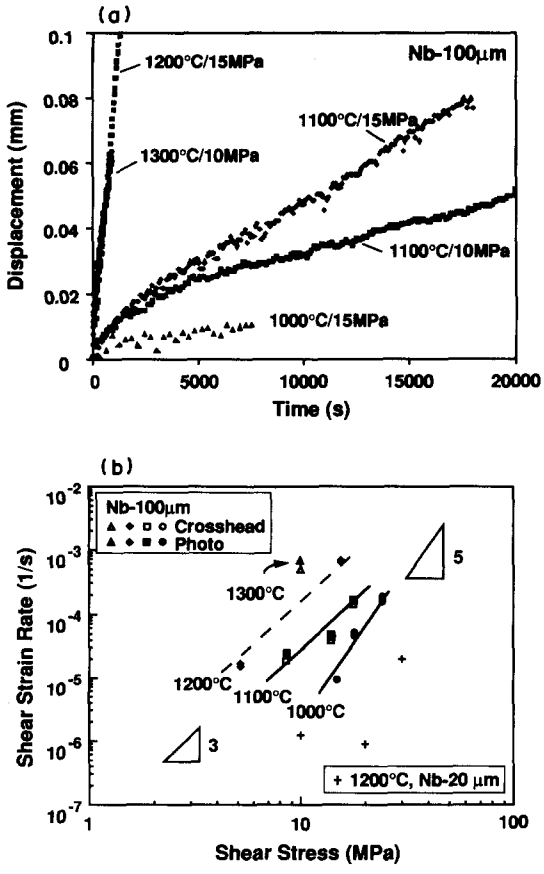

Fig. 5. (a) Displacement vs time curves from several constant load tests with 100 μm-Nb specimens, the tests were interrupted before failure. (b) Steady-state creep rate vs stress for 100 μm-Nb specimens tested at 1000–1300°C, measured from both crosshead displacements and micrographs. One set of data for the 20 μm-Nb specimens at 1200°C are also shown, which illustrates creep rates that are two orders of magnitude lower than that for 100 μm-Nb specimens.

deformation. From the limited data of shear stress and strain rate plotted on a log–log scale, one can estimate the stress exponent (n-value) of the creep equation $\dot{\gamma} = A\tau^n \exp(-Q/RT)$, where $n = 5$ for 1000°C and $n = 3$ for 1100°C and higher. The average activation energy for this temperature range is estimated to be 280 kJ/mol. These results represent only approximate estimates, since there is considerable scatter in the experimental creep data presented. A possible reason for this scatter is the non-planarity of the Nb/Al_2O_3 interfaces after diffusion bonding.

The increase in stress exponent for creep above 1000°C indicates a change in the deformation mechanism. At 1000°C, $n = 5$, this value is typical of dislocation creep [30], and flow lines and substructures as that shown in Fig. 5 are expected to develop. Above 1100°C, diffusional processes provide greater contribution. If a subgrain structure develops during creep, Nabarro–Herring creep of subgrains can occur, and a stress exponent near 3 is expected [31]. For pure Nb, the creep rate under an applied stress of 20 MPa is in the range of 10^{-6} to 10^{-5} s^{-1} [32], which is similar to the shear creep rate found in the present investigation.

3.2.2. Ductile fracture of Nb layer and evolution of microstructural damage Figure 6 shows the side view of a specimen with 100 μm-thick Nb layers that was crept for 10 h at 1200°C under a constant load equivalent to an average shear stress of 10 MPa. The specimen deformed by shear along the mid-plane of the Nb; the two Nb half layers were displaced relative to one another by approximately 250 μm. Despite the severe damage to the Nb, the specimen continued to sustain the applied load up to this stage. The absence of a significant stress normal to the Nb/Al_2O_3 interface prevents separation of the Nb along the highly distorted mid-plane. The ability to sustain load appears to be related to re-joining of the Nb in a fashion analogous to frictional welding.

SEM micrographs showing progressive deformation of the Nb grains in 100 μm Nb/Al_2O_3 specimens during shear testing at 1200°C are given in Fig. 7. Prior to testing, the grain boundaries were flat

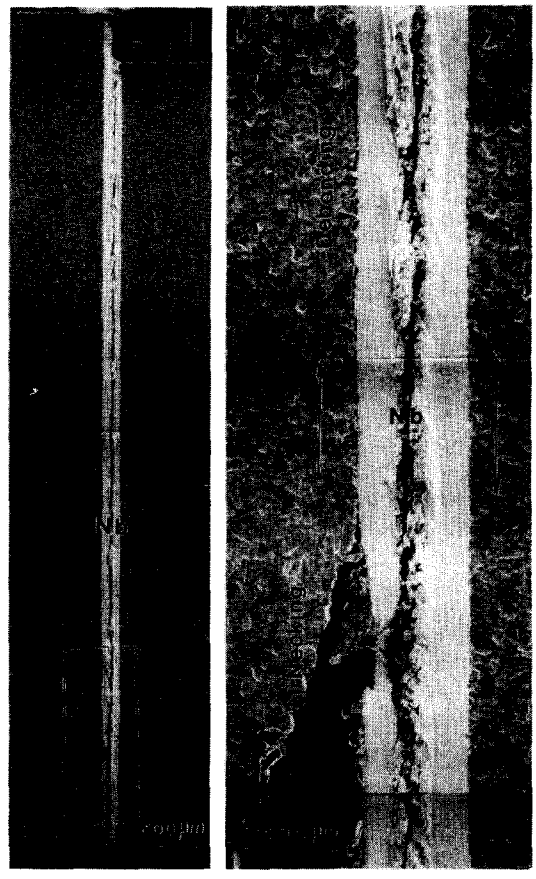

Fig. 6. Micrographs obtained from a 100 μm-Nb specimen crept at 1200°C at 10 MPa for 7 h, (total displacement = 250 μm). Note that limited damage developed within the Al_2O_3, while extensive shear creep and damage developed within the Nb layer. The figure on the right is an enlargement of the inset, showing interface debonding and necking in the Nb.

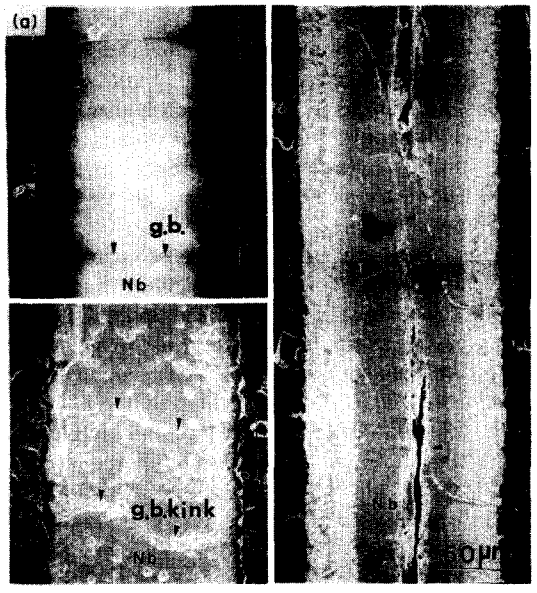

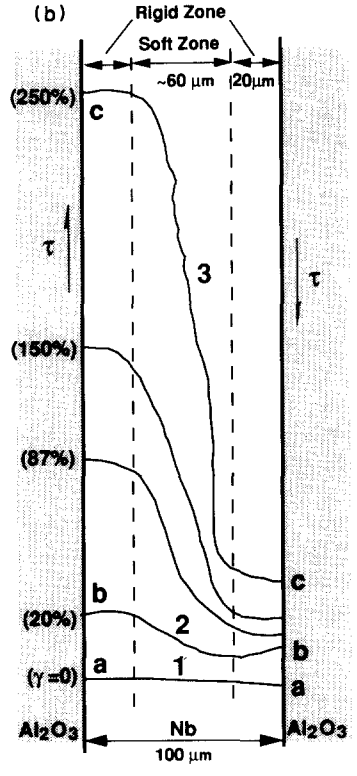

Fig. 7. (a) Micrographs of the 100 μm thick Nb specimens in etched condition (etchant: HNO_3(1.40):HF(40%) = 1:3 (vol), 10 s. The separation at the interface is an artifact of etching). (1) Before test the grain boundaries were flat and perpendicular to the interface; (2) after creep at 1200°C for 2 h (with displacement of 20 μm,) the grain boundaries were kinked into a sigmoidal shape, indicating that the central portion of the Nb experienced more deformation than that near the interfaces; (3) after creep at 1200°C for 7 h (with displacement of 250 μm) extensive grain boundary kinks (see arrows for grain boundaries) and some substructure were formed in the middle portion of the Nb layer. (b) Grain boundary profiles from several creep tests, obtained by a computer scanner on SEM micrographs.

across the entire 100 μm thickness and were parallel to one another [see Fig. 7(1)]. The extent of grain boundary kinking, as well as the relative shear displacement at the top and bottom of the specimens, provided a means to estimate the plastic shear strain that occurred in the Nb layer. After 20% shear strain, the grain boundaries kinked to assume a sigmoidal shape [Fig. 7(2)]. With further displacement, equivalent to 250% shear strain, extensive shear localization and creep damage developed in the center of the Nb-layer; subgrains ($\sim$10 μm size) also developed within the central half-thickness of the Nb [Fig. 7(3)]. This subgrain formation suggests that dislocation mechanism plays an important role in the creep behavior. Traces of the grain boundary profiles from specimens deformed to different displacements are shown in Fig. 7(4). These profiles show that deformation within the Nb layer was extremely inhomogeneous, with only the central 50 μm region participating in the flow process. With an increase in punch displacement, the grain boundary kinks continued to develop until, at large strains, they became discontinuous along the mid-plane of the Nb layers. Close to the Nb/Al_2O_3 interfaces, the Nb grain boundaries exhibited very limited shearing, and remained perpendicular to the interface. This inhomogeneous deformation was prevalent along the entire height dimension of the Nb layer.

3.2.3. Near-interface chemistry and strength. A possible cause of grain boundary kinking is the constraint to shear deformation provided by the surface roughness of the Al_2O_3. However, this constraint would affect the region adjacent to the interface over a distance that is of the same order as the roughness ($\sim$1–3 μm). This distance is much smaller than the rigid region adjacent to the interface over which kinking was not observed. Furthermore, since the specimen breadth was more than 300 times the thickness of the Nb layer, the plastic constraint in the breadth direction [x direction in Fig. 1(a)] cannot vary appreciably through the thickness of the Nb layer. Thus, plastic constraint cannot be responsible for the inhomogeneity of plastic flow observed in the Nb. A detailed FEM analysis of this problem is underway. Preliminary results show an extremely minor effect of such constraint on the shape of the flow lines, if the creep resistance of Nb is assumed constant across the thickness. Thus, plastic constraint effects are believed to be negligible in this special case of pure shear loading.

The most probable mechanism for grain boundary kinking is a variation in the flow behavior within the Nb layers, as a result of compositional changes occurring during diffusion bonding. To examine this possibility, electron microprobe analysis was performed to determine the chemical composition across the thickness of the Nb layer. The relative distribution of [O], [Al], and [Nb] across the interface in a specimen with 100 μm Nb layers is shown in Fig. 8. From the interface to the central portion of the Nb

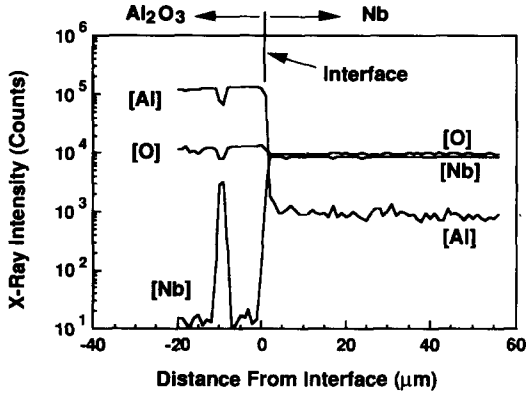

Fig. 8. Relative intensities of X-ray diffraction for [Al], [O], and [Nb] across the Al_2O_3/Nb interface. The sample was diffusion-bonded at 1600°C and 7 MPa for 2 h. The Nb peak in the Al_2O_3 is caused by intrusion into the Al_2O_3.

layer, the aluminum concentration is found to decrease rapidly near the interface, and continue to decrease within the Nb layer, proceeding as far as the mid-plane of the Nb layer. From the quantitative analysis of composition, the aluminum concentration in the Nb phase decreases from 1 at.% in the vicinity of the interface to less than 0.4 at.% at a distance of 50 μm from the interface. This result is consistent with the results obtained from other investigations of the Nb/Al_2O_3 system [33, 34]. The concentration of [Al]- or [O]-containing precipitates in the Nb layers would be proportional to this profile. XRD analysis of the Nb surface from a specimen that was interfacially fractured at room temperature, showed that small amounts of precipitates of Al_2O_3, NbO and $NbO_{2.432}$ were present at the interface (see Fig. 9). Clearly both [Al] and [O] had diffused into Nb during the diffusion bonding cycle, providing a strong chemical bond along the interface. Both the Al in solid solution in Nb and the precipitates can cause a hardening effect near the Nb/Al_2O_3 interfaces. Microhardness measurements further confirmed a hardening effect in the vicinity of the interface, as shown in Fig. 10. Because of strong bonding in this bi-material system and the intrusion of the Nb into the Al_2O_3, the interface strength and toughness are greater than either of the constituents. This surface intrusion eliminates the porosity along the interface and increases the toughness of the interface through the mixing of the brittle phase with the ductile phase.

3.3. Effect of Nb layer thickness

Due to the large distances over which compositional changes can occur near the interface, thinner Nb layers would be less likely to have a pure Nb core. In other words, the effect of near interface strengthening will have a much greater impact on the mechanical behavior of laminates with thin ductile layers. Indeed, there was a dramatic difference between the mechanical behaviors of the composites containing 20 and 100 μm Nb layers. Figure 11(a) shows load vs displacement curves for specimens with 20 μm- and 100 μm-thick Nb layer, and for a specimen of pure Al_2O_3 (without Nb interlayer), under the same constant speed and temperature. Although the specimens with 20 μm Nb layers had a much higher ultimate load than that of the 100 μm-Nb specimens, they had a significantly lower plastic component of displacement. The mechanical behavior and failure mode of the composites with 20 μm Nb layers were, in fact, very similar to the brittle fracture behavior of pure Al_2O_3 specimens. This thickness effect is expected even in the absence of any chemical effect, for ductile layers having a high strain rate sensitivity. For the same displacement rate the thinner Nb layer can experience a shear strain rate which is at least 5 times higher than that for the 100 μm layer Nb sample. Due to the high strain rate sensitivity of Nb, the resulting high stresses can readily damage the brittle Al_2O_3 matrix before significant creep can occur in the thin Nb layer.

The energy absorbed for the specimens with thick and thin Nb layers and for pure Al_2O_3 is shown in Fig. 11(b). The energy was calculated by integrating the plots in Fig. 11(a) over the corresponding displacement to obtain the total external work, and then subtracting the associated elastic work due to machine compliance. The 100 μm-Nb specimen has a much higher plastic energy than the 20 μm-Nb specimen and the Al_2O_3, while the latter two have nearly the same behavior. This result indicates that the use of thick Nb layers can increase the toughness of ductile-phase reinforced brittle-matrix composites, while layers thinner than 20 μm may not have significant effect.

SEM micrographs showing the fracture path in a 20 μm-Nb/Al_2O_3 specimen and a pure Al_2O_3 specimen are given in Fig. 12. These specimens had very similar damage modes. Multiple crack branching was not observed either in the thinner Nb specimens or in the Al_2O_3 specimens, and the crack follows a path near the line joining the two notches. This is in contrast to the ductile fracture process observed in the 100 μm Nb/Al_2O_3 specimens. With a thin Nb layer, the specimens exhibited brittle behavior, with no significant shear in the Nb layer. Thus, there exists a critical thickness of Nb for toughness enhancement, which is dependent on diffusion bonding parameters.

3.4. Interface fracture

For the diffusion bonding conditions used in this work, the Nb/Al_2O_3 interfaces were strong, and interface debonding and fracture were rarely seen. In a few cases, however, local interface debonding did occur, as shown in Fig. 13, possibly because of local contamination of the Nb sheets. Interface debonding was also observed near the tool contacts, and during the last stage of crack propagation, as the main crack from the top and bottom of the specimen merged near the center of the specimen. Clearly normal stresses are generated in this area. The interface in the thinner Nb specimens were found to debond

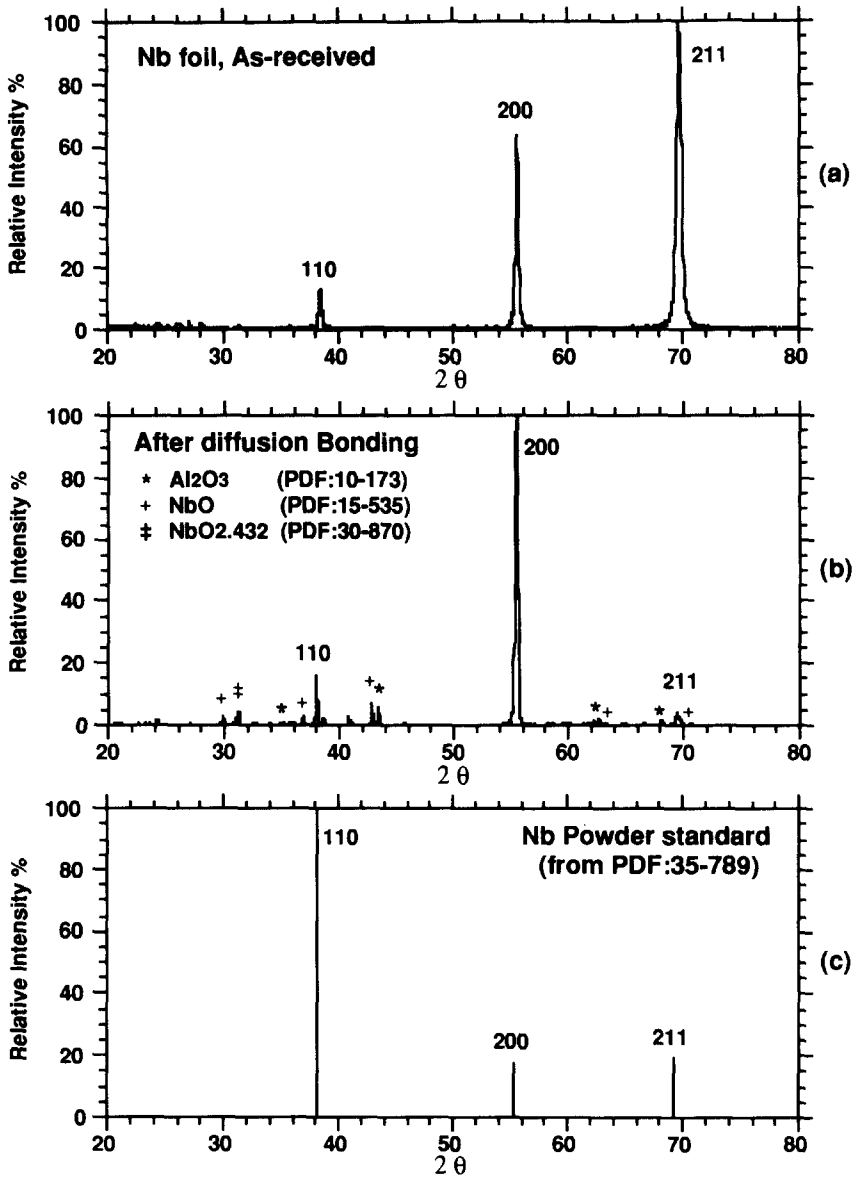

Fig. 9. X-ray diffraction patterns: (a) as-received Nb foil normal to the surface; (b) Nb-surface after diffusion-bonding, the specimen was interfacially fractured at RT, and a small amount of Nb oxides were detected; (c) Nb powder standard. The difference in X-ray intensities in (a) and (b) are probably due to the variation in cold-rolling vs annealing textures.

somewhat easier than those with the 100 μm-Nb, possibly because the thin Nb layer offered greater resistance to deformation and could not relieve local stress build-up by plastic deformation as in the thicker Nb specimen. Thus, the interfacial strength in Nb/Al_2O_3 interfaces are typically greater than the cohesive strength of Al_2O_3 and the constrained flow strength of Nb. The interdiffusion at Nb/Al_2O_3 interface is a key to this strength enhancement.

3.5. Overall composite fracture process and transition behavior

In this study, three basic damage mechanisms were observed: (a) brittle fracture within the Al_2O_3 (intergranular fracture); (b) ductile fracture within the Nb layer (creep rupture); (c) brittle fracture along the Nb/Al_2O_3 interface. These three damage mechanisms operate simultaneously, in a competitive manner; the overall fracture behavior of the composite depends upon the dominant mechanism. Since the relative contribution of each process varies with temperature, applied stress, and the Nb thickness, there are three distinct regimes of composite behavior, as illustrated schematically in Fig. 14. These are described below:

Regime 1. Ductile fracture. At high temperatures and low applied stresses (below the fracture stress of the Al_2O_3), damage is restricted within the Nb layer, with pronounced shear deformation occurring along the mid-plane of the Nb. The shear deformation is followed by cavitation, slow crack growth and

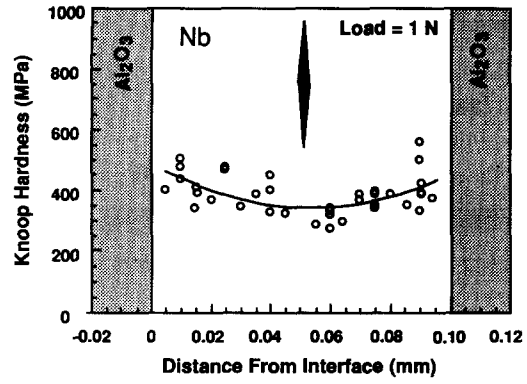

Fig. 10. Room temperature microhardness across the thickness of the 100 μm-Nb layer. Note that the central portion of the Nb is softer than the region near the interfaces.

linkage. Concurrently, a re-joining of the fractured pairs occurs even after linkage of small shear cracks in the mid-plane of Nb during the shear creep.

Regime 2. Brittle fracture within Al_2O_3 or along the interfaces. This fracture mode was observed at high stresses and low test temperatures, and also when a high normal stress develops across the interface. This occurred more often for specimens with thinner Nb layers.

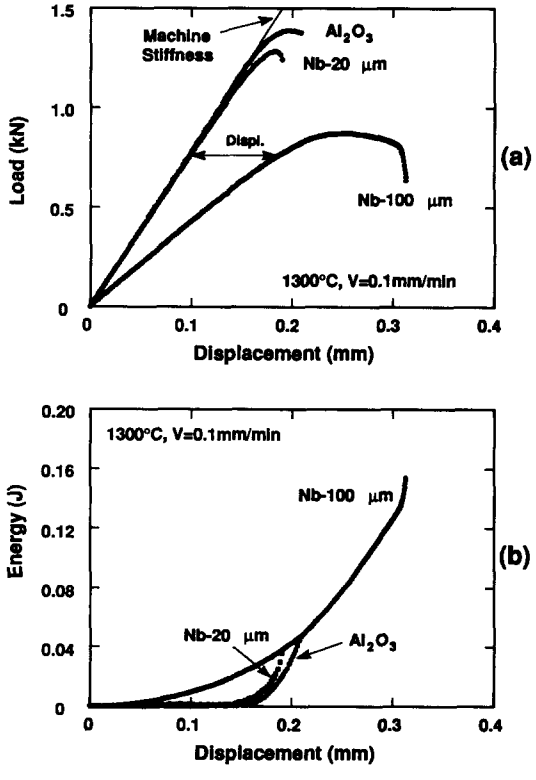

Fig. 11. (a) Load vs displacement curves for specimens with 100 μm and 20 μm-Nb layers, and for pure Al_2O_3 specimen. The curves were obtained at 1300°C at a constant speed of 0.1 mm/min; (b) energy vs displacement, corresponding to the curves shown in (a).

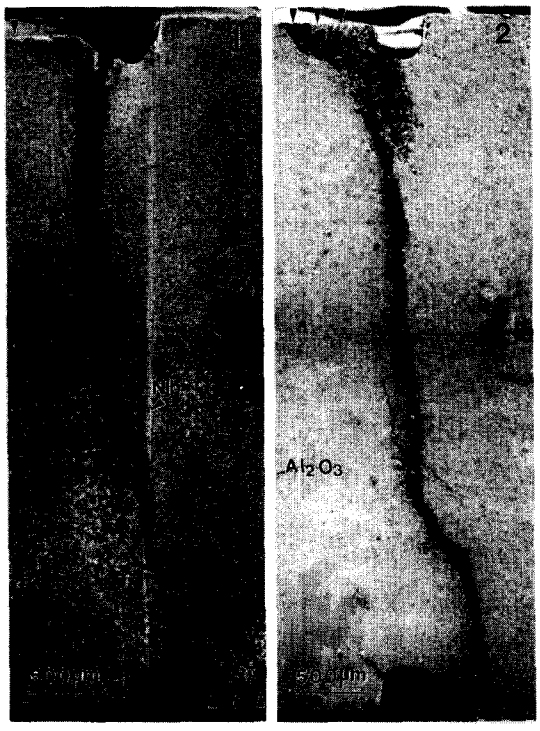

Fig. 12. Front view of specimens showing fracture path: (1) 20 μm-Nb specimen, and (2) Al_2O_3 (without Nb layer). The test conditions are given in Fig. 11.

Regime 3. Transitional fracture. Multiple energy dissipating mechanisms may be active within this regime. Brittle fracture within the Al_2O_3 is concurrent with plastic flow within the Nb phase, and crack branching toward the Nb/Al_2O_3 interface. At elevated temperatures and under shear loading, the presence of a relatively thick (100 μm) Nb layer causes a redistribution of the stress within the Al_2O_3 matrix and attracts the crack toward the interface

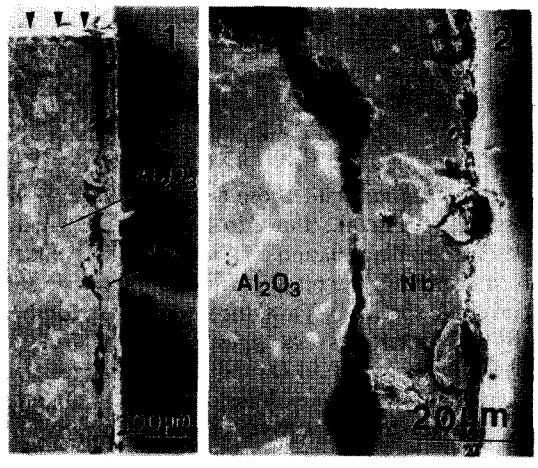

Fig. 13. Front view of 20 μm-Nb specimen showing interface debonding after testing at 1200°C under a constant displacement rate of 0.1 mm/min: (1) low magnification; and (2) high magnification showing that interface debonding is discontinuous. Note that only one-half of the specimen is shown.

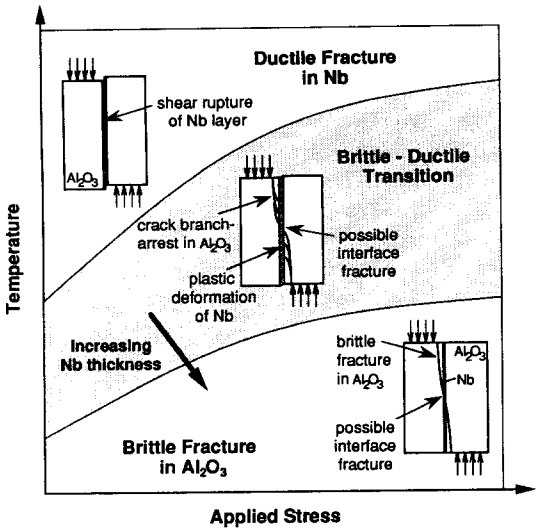

Fig. 14. Schematic illustration of three regimes of Nb/Al_2O_3 laminate fracture behavior under shear loading, as functions of temperature, applied stress, and the Nb thickness. Between a ductile regime at high temperature-low stress and a brittle regime at low temperature-high stress, there exists a brittle–ductile transition regime (shadowed region). In this regime multiple crack branching in Al_2O_3 with concurrent shear deformation within Nb layer results in additional energy dissipation. As the Nb thickness increases, the ductile fracture regime expands to lower temperature-higher stress region.

prematurely. This stress redistribution occurs due to plastic deformation within the Nb. Because of the extremely strong Nb/Al_2O_3 interface, interfacial debonding does not occur; rather, multiple crack arresting/branching to the interface is observed within Al_2O_3.

In addition to temperature and stress, the Nb thickness plays an important role in the brittle–ductile transition. Composites with Nb-layers as thin as 20 μm showed no increase in toughness over monolithic Al_2O_3, exhibiting a brittle failure mode. Thus, a decrease in Nb thickness can expand the brittle fracture regime, and concurrently reduce the transition and the ductile fracture regimes. Alternatively, increasing the Nb thickness can expand the ductile regime and possibly the transition regime as well.

The fracture path and fracture transition can be influenced by the relative characteristics of the individual constituents and their interface. Studies of the fracture behavior of ceramics [35] indicate that processing-related flaws provide crack initiation sites and control the fracture stress of the Al_2O_3 phase. At room temperature the fracture stress of Al_2O_3 is typically lower than that for Nb, and also lower than the fracture stress of the Nb/Al_2O_3 interface. However, at 1000–1300°C Nb is softer and undergoes plastic flow. The flow stress of Nb is dependent on the strain rate or applied stress. At high temperatures the strength of Al_2O_3 and the interface may also decrease somewhat, but not as much as that of Nb. Since failure of the composite is controlled by weakest path, higher temperature and lower applied stress favor ductile fracture within Nb, alternatively, lower temperature and higher applied stress favor brittle fracture within Al_2O_3, and probably at interface as well. For the present composite system, if the applied stress is above 40 MPa, damage in the Al_2O_3 develops very rapidly, and the specimen fails in a brittle manner within several minutes of loading. During this period, Nb also creeps, but due to its higher ductility Nb can sustain very large strains prior to failure. If the applied stress is below approximately 40 MPa, limited creep damage occurs in the Al_2O_3, but Nb undergoes significant creep deformation. Failure therefore occurs either within the Al_2O_3 or within the Nb, and the transition from one to the other will depend on the applied stress and testing temperature.

4. ADDITIONAL INSIGHTS: FRACTURE MODE MIXITY IN THE SHEAR TEST

It is realized that the exact loading condition in the present shear test is complicated and can deviate from one of pure shear. The complexity arises from both the mismatch of the bi-material constants and the complicated stress state developed during the experiments. The influence of material mismatch on mode mixity can be assessed from an analysis by Rice [36]. From this analysis, the stress intensity factor in a bi-material containing a thin layer, $K_1 + iK_2$, is related to $K_I + iK_{II}$ of a homogeneous material (without the layer) by a phase angle shift ω

$$\tan^{-1}(K_2/K_1) = \tan^{-1}(K_{II}/K_I) + \omega \qquad (1)$$

where, ω is a function of α and β, the modulus mismatch parameters of Dundurs [37] (these parameters are related to the Young's modulus and Poisson's ratio of both constituents). In most engineering materials ω ranges between 5° and −18°.

Even neglecting the phase shift effect, pure shear is not easy to obtain, due to the tool contact, punch-die clearance and specimen geometry effect. For bend tests, for example, curvature and stress gradients develop naturally. For the punch apparatus used here, the punch shear test can be considered as an extreme case of bending of a thick beam, where the locations of the concentrated loads at the inner and outer spans are very close along the beam axis. In case of a large outer span, the stress along the interface can be approximately determined by considering a homogeneous beam subjected to elastic bending, and multiplying by a stress concentration factor. For simple bending of a notched bar, the normal and shear stresses can be expressed as [38]

$$\sigma_{11} = m_1 \frac{6Ps}{H'^3 W} y \qquad (2)$$

$$\sigma_{12} = m_2 \frac{3}{2} \frac{P/2}{WH'} \left\{ 1 - \left(\frac{2y}{H'} \right)^2 \right\} \qquad (3)$$

where, m_1 and m_2 are the stress concentration factors due to the notch, y is the vertical distance from the specimen center, a is the notch depth, H and W are the specimen height and width, and $H' = H - 2a$, see Fig. 1. Dimensionally, σ_{11} is proportional to s but σ_{12} is independent of s; accordingly the stress intensities K_I and K_{II} at a notch should follow the same trend. Therefore, the phase angle $\Psi[= \tan^{-1}(K_{II}/K_I)]$ monotonically decreases with the clearance s. For small s, the bending solution is no longer valid, since a complicated stress state exists in the vicinity of the tool contact points, which causes both shear and normal stresses. Preliminary results obtained from finite element analysis [39], indicate that at room temperature tensile stresses are generated near the point of contact. However, by the introduction of notches this effect can be minimized and Ψ can approach $\pi/2$ for a large part of specimen. The presence of a ductile layer imparts uniform applied shear traction along the interface, as shown in Fig. 3(b), which can change Ψ at the crack tip to approach a value of $\pi/4$ within Al_2O_3.

It is worth noting that in certain circumstances the existence of a stress component normal to interface may prove to be an advantage for the punch-shear test. From equations (2) and (3), the phase angle Ψ can be varied from $\pi/2$ toward zero by increasing s/H' from 0 to $\gg 1$. This allows one to study the effect of mode mixity on interface debonding and composite fracture using the same experimental configuration.

It has been reported by Rühle *et al.* [18] that at room temperature interface fracture in Nb/Al_2O_3 composites can occur under Mode-I loading with a high crack velocity, and an increase in K_{II}/K_I ratio will increase the interface fracture energy [22, 24]. The results of the present investigation show that at elevated temperature the interface fracture of Nb/Al_2O_3 system generally does not occur for Mode-II loading. In addition to strong interface bonding in the Nb/Al_2O_3 system, the non-planarity of the interface, arising from surface roughness of Al_2O_3, may be partially responsible for the absence of debonding. In order to shear a rough interface a great deal of plastic energy is required to cut through the nonplanar Nb steps, which is not necessary for Mode-I fracture.

5. CONCLUSIONS

A simple experimental technique was developed to study the elevated-temperature creep and fracture behavior of brittle matrix laminates containing ductile phases under shear loading. As a result of the experimental study, an understanding of the high temperature toughening mechanisms and brittle-to-ductile transition in these materials were developed. The primary findings of this study are listed below:

1. The addition of a ductile Nb layer to Al_2O_3 modified the fracture mode from one of brittle fracture to that exhibiting additional modes of energy dissipation. For shear loading parallel to the Nb/Al_2O_3 interfaces, these modes are: (i) multiple crack branching within the Al_2O_3, towards the Nb/Al_2O_3 interface, (ii) debonding along the Nb/Al_2O_3 interface, and (iii) plastic flow and shear cracking within the Nb layer. Multiple crack branching to the interface is attributed to the accommodation of displacement by plastic deformation of the Nb-layer, which causes stress redistribution within the Al_2O_3. The extensive crack branching within the Al_2O_3 and concurrent shear creep within the Nb are mechanisms for enhanced toughening in these laminates.

2. The fracture path was controlled by the applied stress and temperature, and the thickness of the Nb layer. High stresses favor brittle fracture within the Al_2O_3, while low stresses favor shear creep and ductile fracture within the Nb. A brittle/ductile transition occurred at an average shear stress of about 40 MPa. Interface fracture was rarely observed for this strongly bonded bi-material system.

3. Based upon limited data for creep rate, the stress exponent for creep of the constrained Nb layer decreased from approximately 5 at 1000°C to approximately 3 at temperatures from 1100 to 1200°C. The different stress exponents indicate a change in the dominant creep deformation mechanism, from dislocation controlled creep to possibly diffusion assisted subgrain creep.

4. Microstructural examination revealed that the initial flat Nb grain boundaries underwent considerable kinking as a consequence of inhomogeneous creep across the Nb thickness. This inhomogeneous creep was attributed to aluminum and oxygen diffusion from the Al_2O_3 into the Nb during diffusion bonding, which increased the creep resistance of Nb in the vicinity of the interfaces.

5. The Nb thickness had a significant effect on the fracture process. For thinner layers of Nb the entire layer can be strengthened by interdiffusion of Al and O. Furthermore, since a thinner layer experiences a higher local strain rate than a thicker layer, it supports a higher stress level. Composites with thinner 20 μm Nb layers exhibited poor ductility. The fracture path for these composites was similar to that found in monolithic Al_2O_3, indicating brittle behavior. Ductile phase toughening showed a marked enhancement when the Nb layer thickness was increased to 100 μm.

REFERENCES

1. L. S. Sigl, A. G. Evans, P. Mataga, R. M. McMeeking and B. J. Dalgleish, *Acta metall.* **36,** 945 (1988).
2. B. D. Flinn, M. Rühle and A. G. Evans, *Acta metall.* **37,** 3001 (1989).
3. P. A. Mataga, *Acta metall.* **37,** 3349 (1989).
4. H. C. Cao, B. J. Dalgleish, H. E. Dève, C. Elliott, A. G. Evans, R. Mehrabian and G. R. Odette. *Acta metall.* **37,** 2969 (1989).
5. T. C. Lu, A. G. Evans, R. J. Hecht and Mehrabian, *Acta metall. mater.* **39,** 1853 (1991).

6. M. Bannister, H. Shercliff, G. Bao, F. Zok and M. F. Ashby, *Acta metall. mater.* **40,** 1995 (1992).
7. R. O. Ritchie, R. M. Cannon, B. J. Dalgleish, R. H. Dauskaskardt and J. M. M. McNaney, *Mater. Sci. Engng.* Submitted.
8. T. S. Oh, J. Rödel, R. M. Cannon and R. O. Ritchie, *Acta metall.* **36,** 2083 (1988).
9. R. M. Cannon, B. J. Dalgleish, R. H. Dauskaskardt, T. S. Oh and R. O. Ritchie, *Acta metall. mater.* **39,** 2145 (1991).
10. P. G. Charalambides, J. Lund, R. M. McMeeking and A. G. Evans, *J. appl. Mech.* **111,** 77 (1989).
11. B. J. Dalgleish, M. C. Lu and A. G. Evans, *Acta metall.* **36,** 2029 (1988).
12. B. J. Dalgleish, K. P. Trumble and A. G. Evans, *Acta metall.* **36,** 1923 (1989).
13. H. C. Cao, M. D. Thouless and A. G. Evans, *Acta metall.* **36,** 2037 (1988).
14. R. O. Ritchie, R. M. Cannon, B. J. Dalgleish, R. H. Dauskaskardt and J. M. M. McNaney, *Mater. Sci. Engng.* Submitted.
15. N. P. O'Dowd, M. G. Stout and C. F. Shih, *Phil. Mag. A* **66,** 1037 (1992).
16. N. P. O'Dowd, C. F. Shih and M. G. Stout, *Int. J. Solids Struct.* **29,** 571 (1992).
17. K. S. Kim and N. Aravas, *Int. J. Solids Struct.* **24,** 417 (1988).
18. M. Rühle, K. Burger, W. Mader and A. G. Evans, in *Fundamentals of Diffusion Bonding, Proc. First Seiken Int. Symp. on Interface Structure, Properties and Diffusion bonding*, Tokyo, Japan, 1985 (edited by Y. Ishida), pp. 43–88. Elsevier, Amsterdam (1987).
19. G. E. Beltz and J.-S. Wang, *Acta metall. mater.* **40,** 1675 (1992).
20. W. Mader and G. Necker, in *Metal–Ceramic Interfaces, Proc. Int. Workshop*, Santa Barbara, Calif. (edited by M. Rühle *et al.*), pp. 222–233. Pergamon Press, Oxford (1989).
21. W. Mader and M. Rühle, *Acta metall.* **37,** 853 (1989).
22. S. Suresh, C. F. Shih, A. Morrone and N. P. O'Dowd, *J. Am. Ceram. Soc.* **73,** 1257 (1990).
23. N. P. O'Dowd, C. F. Shih and M. G. Stout, *Int. J. Solids Struct.* **29,** 571 (1992).
24. J. W. Hutchinson, in *Metal–Ceramic Interfaces, Acta–Scripta Metall. Proc. Ser. 4* (edited by M. Rühle *et al.*), pp. 295–306. Pergamon Press, Oxford (1990).
25. T. S. Oh, R. M. Cannon, J. Rödel, A. M. Glaeser and R. O. Ritchie, in *Interfaces in Polymer, Ceramic, and Metal Matrix Composites* (edited by H. Ishida), pp. 567–581. Elsevier, Amsterdam (1988).
26. T. J. Mackin, P. D. Warren and A. G. Evans, *Acta metall. mater.* **40,** 1251 (1992).
27. R. M. Cannon, B. J. Dalgleish, R. H. Dauskasardt, T. S. Oh and R. O. Ritchie, *Acta metall. mater.* **39,** 2145 (1991).
28. *Metal Handbook*, Vol. 2, 9th edn, p. 778. ASM, Metal Park, Ohio (1979).
29. W. R. Cannon and T. G. Langdon, *J. Mater. Sci.* **23,** 1 (1988).
30. M. F. Ashby, *Acta metall.* **20,** 887 (1972).
31. T. H. Courtney, *Mechanical Behavior of Materials*, p. 277. McGraw-Hill, New York (1990).
32. L. P. Jahnke, in *High Temperature Materials II, Metall. Soc. Conf.*, Cleveland, Ohio, 1961 (edited by G. M. Ault *et al.*), Vol. 18, p. 283. Interscience, New York (1963).
33. K. Burger and M. Rühle, *Ultramicroscopy* **29,** 88 (1989).
34. M. Rühle and W. Mader, in *Design Interface for Technological Applications* (edited by S. D. Peteves), p. 145–95.
35. A. G. Evans, *J. Am. Ceram. Soc.* **65,** 127 (1982).
36. J. R. Rice, *J. appl. Mech.* **55,** 98 (1988).
37. J. J. Dundurs. *J. appl. Mech.* **36,** 650 (1969).
38. F. P. Beer and E. R. Johnson Jr, in *Mechanics of Materials*, Chaps 4 and 5, pp. 150–188. McGraw-Hill, New York (1981).
39. C. N. Ma, X. Wu, A. K. Ghosh and J. W. Holmes, unpublished work on FEM of shear test (in progress).